PNAS RESEARCH ARTICLE | CHEMISTRY

Atomic distribution and local structure in ice VII from in situ neutron diffraction

Keishiro Yamashita[a,1,2], Kazuki Komatsu[a], Stefan Klotz[b], Oscar Fabelo[c], Maria T. Fernández-Díaz[c], Jun Abe[d], Shinichi Machida[d], Takanori Hattori[e], Tetsuo Irifune[f], Toru Shinmei[f], Kazumasa Sugiyama[g], Toru Kawamata[g], and Hiroyuki Kagi[a]

Edited by Russell Hemley, University of Illinois at Chicago, Chicago, IL; received May 27, 2022; accepted September 02, 2022

Ice polymorphs show extraordinary structural diversity depending on pressure and temperature. The behavior of hydrogen-bond disorder not only is a key ingredient for their structural diversity but also controls their physical properties. However, it has been a challenge to determine the details of the disordered structure in ice polymorphs under pressure, because of the limited observable reciprocal space and inaccuracies related to high-pressure techniques. Here, we present an elucidation of the disordered structure of ice VII, the dominant high-pressure form of water, at 2.2 GPa and 298 K, from both single-crystal and powder neutron-diffraction techniques. We reveal the three-dimensional atomic distributions from the maximum entropy method and unexpectedly find a ring-like distribution of hydrogen in contrast to the commonly accepted discrete sites. In addition, total scattering analysis at 274 K clarified the difference in the intermolecular structure from ice VIII, the ordered counterpart of ice VII, despite an identical molecular geometry. Our complementary structure analyses robustly demonstrate the unique disordered structure of ice VII. Furthermore, these findings are related to proton dynamics, which drastically vary with pressure, and will contribute to an understanding of the structural origin of anomalous physical properties of ice VII under pressures.

ice | high pressure | neutron diffraction | disordered structure

Significance

Ice VII is a textbook example of a hydrogen-disordered solid, but the exact distribution of hydrogen atoms is still unknown. Here, we report the detailed atomic distribution and local structure of ice VII revealed from neutron-diffraction data of both single-crystalline and powder specimens under high pressure. Recent technical developments enabled a robust analysis of the diffraction data: ice VII has a different intermolecular structure from its ordered counterpart, ice VIII, even at short distances, despite their identical molecular geometry. Moreover, hydrogen has an unusual ring-like distribution and an elongation toward hydrogen-bonded water molecules. Our findings highlighted the uniqueness of the disordered structure of dense ice and open the door for further understanding of network structure in extreme conditions.

Water freezes into various solid structures, including crystalline and noncrystalline phases, when compressed or cooled down. Ice VII is one of its 20 crystalline phases and is stable at room temperature between 2 and 60 GPa. In this pressure range, ice VII shows various anomalous behaviors related to pressure-dependent proton dynamics, such as a sharpening of the Raman peak of its symmetric vibration mode at 11 to 13 GPa (1) which is caused by a crossover of dominant processes from molecular rotation to proton translation (2, 3). Ice VII also undergoes a phase transition involving hydrogen-bond symmetrization toward ice X (4, 5). This anomalous crystalline phase has attracted much scientific interest, and it hence appears crucial to understand its detailed structure.

The structure of ice VII can be regarded as two interpenetrating, diamond-like networks formed by hydrogen-bonded water molecules (Fig. 1*A*). In each network, water molecules are orientationally disordered as those in other ice polymorphs (e.g., ordinary ice [ice I_h]) (6). Hydrogens of each water molecule randomly occupy two of four sites toward the neighboring oxygens. In other words, the overall structure of ice VII consists of a combination of various configurations. Ice VII transforms into ice VIII by ordering the hydrogen positions (or molecular orientations) at low temperatures (<273 K at 3 GPa (7)). In ice VIII, the orientations of water molecules are well defined: hydrogens occupy two particular sites, and molecular orientations between the interpenetrating networks are aligned antiparallel along the *c*-axis, which induces displacement of the network relative to the other along the *c*-axis. This results in a tetragonal distortion of ice VIII.

The disordered structure of ice VII is generally represented by a cubic unit cell with space group $Pn\bar{3}m$ (#224) in which oxygens locate at 2*a* site and hydrogens at 8*e* site with occupancy of 0.5 (hereafter, this model is called a single-site model). The symmetric constraints simplify the structure model as it needs only one parameter for the hydrogen position (*x*, *x*, *x*) and two variables for atomic displacement parameters (ADPs) (three for anisotropic ADPs). The single-site model reproduces well the diffraction patterns and, therefore, has been adopted in almost all previous studies (8, 9). Nevertheless, structure refinements based on the single-site model are known to cause a highly anomalous geometry of the water molecule (e.g., an unrealistically short O-D covalent bond length [0.89 Å (10)]) compared with those in ice VIII (0.97 Å) (10, 11), whereas a computational study showed similar distances for both phases (12).

Author contributions: K.Y., K.K., and H.K. designed research; K.Y., K.K., S.K., O.F., M.T.F.D., J.A., S.M., and T.H. performed research; T.I., T.S., K.S., and T.K. contributed new materials/analytic tools; K.Y. and K.K. analyzed data; K.Y. wrote the paper; and H.K. directed the research.

The authors declare no competing interest.

This article is a PNAS Direct Submission.

[1]Present address: Institute of Physical Chemistry, University of Innsbruck, Innrain 52c, 6020 Innsbruck, Austria.

[2]To whom correspondence may be addressed. Email: Keishiro.Yamashita@uibk.ac.at.

This article contains supporting information online at http://www.pnas.org/lookup/suppl/doi:10.1073/pnas.2208717119/-/DCSupplemental.

Published September 26, 2022.

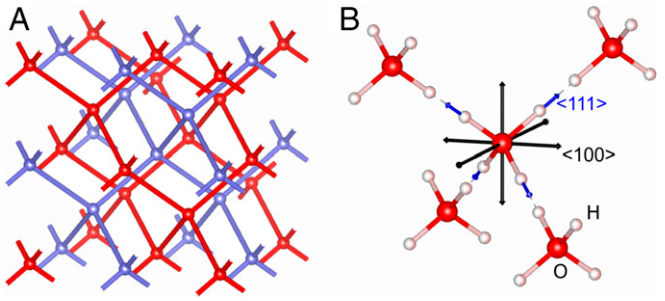

Fig. 1. Crystal structure of ice VII. (*A*) Interpenetrating, diamond-like, hydrogen-bonding networks colored in red and light blue. Balls on the nodes correspond to oxygen, while hydrogen is omitted for clarity. (*B*) Close-up view of water molecules in the same hydrogen-bonding network. Large red and small pink balls correspond to oxygen and hydrogen, respectively.

This implies that water molecules in ice VII are not in the positions assumed in the single-site model. The agreement of the single-site model with the diffraction patterns appears to be a result of time and spatial averaging in diffraction measurements.

On the other hand, more reasonable "multi-site" models have been proposed to date to describe the real structure of ice VII. In these models, the hydrogen atoms are located away from a straight line between adjacent oxygens, especially toward the three nonbonded oxygens belonging to the other hydrogen-bonding network (13). Oxygen positions were modeled mainly in two ways: displacements toward <111> (14) or <100> (10), as illustrated in Fig. 1*B*. Displacements along <100> imply that ice VII favors local structures similar to those in the ordered structure of ice VIII, while displacements along <111> imply the opposite. The <111> model entails differences in hydrogen-bond length: a shorter one in which one oxygen gets close to the neighbor and a longer one in which oxygen is away from the neighbor (14). The existence of the bimodal probability of hydrogen-bond length is still controversial (15, 16). However, no unambiguous structure refinements have been achieved so far, because the atomic displacements from the single-site position are very small (0.1 Å) and this parameter strongly correlates with ADPs in the structure refinement. A computational study from density functional theory suggested a probability distribution similar to the <100> displacement of oxygen rather than <111>, although it also insisted that both displacement models are too simplistic (17). In conclusion, the actual structure in ice VII has not been experimentally proven up to the present.

Here, we report in-situ single-crystal neutron diffraction using a newly developed apparatus. Previous powder diffraction studies had limitations in resolution related to peak duplicates in one-dimensional diffractograms, whereas single-crystal diffraction can directly provide discrete reflection intensities without peak overlap and can lead to a definitive conclusion by double-checking with the well-established powder diffraction technique (18). In addition to the technical improvements in measurements, nonconventional analytical approaches are also necessary to reveal the detailed disordered structure of the dense ice without constraints from structure models like the single-site model, because conventional analyses have considerable difficulties in modeling the real distribution. We applied a maximum entropy method (MEM) analysis to reveal three-dimensional atomic distributions in the unit cell. Moreover, information on local structures like the water geometry was extracted as interatomic correlation by total scattering analysis. For these approaches, neutron diffraction is suitable for this study, owing to its sensitivity to hydrogen (deuterium). The scattering length does not decay according to $\sin\theta/\lambda \propto 1/d$, in contrast to X-ray diffraction. Therefore, numerous reflections are observable even for low d-spacing, which allows a structure analysis with high resolution in real space. Deuterated samples (D_2O) were used in all the experiments instead of light water (H_2O) to avoid incoherent scattering. This isotope replacement shifts the phase boundary between ices VI and VII toward slightly lower pressure but does not affect significantly the disordered structures investigated in this study.

Results

The MEM analysis is based on the principle of maximum entropy, a part of Bayesian statistics, which expects the most probable density distribution to be one with the largest information entropy under constraints on the observed structure factors F_o and their uncertainties σF_o.

Results of MEM analyses on both single-crystal and powder diffraction data show ring-like distributions of deuterium around the <111> axes, in the direction toward the oxygen of hydrogen-bonded water, away from the position assumed in the single-site model (Fig. 2 *A* and *B*), and the ring is slightly distorted to a triangular shape. Their maxima are displaced from the axes by 0.1 to 0.2 Å. These are similar to the reported values (13, 14), but such a ring-like distribution can only be approximately described by the displacement ellipsoid conventionally used in least-squares structure refinements. The corners of the triangular-like distribution are in staggered directions to other deuterium sites covalently bonded to the oxygen, as previously suspected (13). In Fig. 2 *C* and *D*, the distance between the maxima of density assigned to deuterium and the average oxygen site is shorter than a plausible covalent O-D bond length of 0.97 Å, as found in ice VIII (10, 11). This explains that the conventional structure analysis using the single-site model results in a shorter (average) O-D covalent bond, whereas the deuterium in ice VIII does not show such spreading distribution (*SI Appendix*, Fig. S4).

On the other hand, oxygens show more elongated distributions toward the O-D covalent bond (Fig. 2 *C* and *D*), which corresponds to <111> direction in the ice VII structure rather than <100> or <110> directions. However, the density distributions are not tetrapodal but pyramidal, meaning that other components, such as along <100>, are not fully excluded. The real disordered structure would be the combination of dominant displacements toward <111> and some other components with variations. The more diffuse features in the single-crystal data compared with the powder data would be mainly due to the achieved resolution for the observed diffractions. Nonetheless, our examinations from two distinct experimental setups, at different neutron sources, with different high-pressure devices and different detectors, suggest the feature of <111> displacement of oxygen is real and intrinsic for ice VII. This is, hence, consistent with the model proposed by Nelmes et al. (14).

These displacements of oxygen and deuterium were partly proposed in the previous studies (13, 14), but our study shows unambiguously the three-dimensional distribution in ice VII by the model-independent MEM approach. Our result shows that the structure of ice VII is clearly distinct from the single-site model. The ring-like distribution of deuterium can be ascribed to the time and spatial average of water molecules in different orientations rather than a distortion of water molecules themselves, like intramolecular bending. Such displacement induces

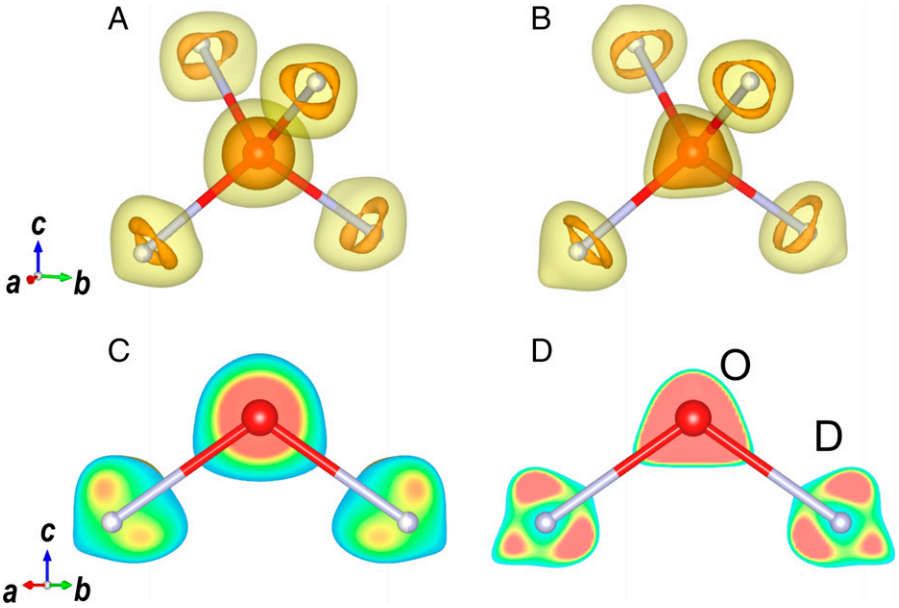

Fig. 2. Distribution of scattering-length density in ice VII derived from (*A*) single-crystal data and (*B*) powder diffraction data, both at 298 K and 2.2 GPa. (*C* and *D*) are cross sections of (*A* and *B*) on the (110) plane, respectively. The oxygens and deuteriums are illustrated as those in the single-site model with O-D = 0.97 Å, as in the water molecule, and ∠DOD = 109.47° for comparison. Density decreases from red to blue color.

bending of the hydrogen-bonding networks from an ideal diamond-like network with cubic symmetry.

It should be noted that the density distribution of deuterium also elongates toward oxygens of the neighboring water molecules. This suggests two possibilities. One explanation is that hydrogen-bonded water molecules get closer, which means the network structure is modified. The other explanation is that the interpenetrating hydrogen-bonding network locally displaces along <111>. This would mean that the local structure of ice VII differs from that of ice VIII, the hydrogen-ordered phase, with displacement along <100>.

Relating to the displacement of oxygen along the <111> direction, a modulated structure was previously proposed from single-crystal X-ray diffraction (19, 20). In our single-crystal neutron diffraction, however, no superlattice reflection was observed similar to any other studies using powder X-ray and neutron diffraction. There is no technical reason why such reflections cannot be observed in our experiment, because the intensity of the superlattice reflection should be comparable to that of 111 reflections (see Fig. 2 in ref. 19), which were observed in our study. The origin of the previously reported superlattice reflection remains, hence, unclear.

In order to reveal the short-range structures of ice VII, such as interatomic distances and local ordering, the correlation functions were derived from the total scattering of powder diffraction instead of extracted intensities of the Bragg peaks, as in the conventional structure refinements and the MEM analysis. The exact O-H(D) distance in ice I_h was derived from the total scattering analysis (21).

The total correlation functions $T(r)$ of ice VII and VIII from powder diffraction at 274 K and 2.2 GPa have a similar profile in the short-r region (Fig. 3 *A* and *B*). Assuming that each correlation has Gaussian-type distribution, $T(r)$ can be divided into several peaks. The representative geometries are listed in Table 1 with corresponding geometry obtained by the Rietveld analysis using the single-site model. The Rietveld analysis resulted in the O-D length of 0.9163 (5) Å in ice VII, significantly shorter than that of 0.9681 (8) Å in ice VIII, which agrees well with previously reported values (10, 11). Our fitting of $T(r)$ gave an O-D distance of 0.9662 (5) Å for ice VII, proving the suggested similarity of its intramolecular structure with ice VIII (22). The coordination numbers of the covalent O-D were estimated to be 1.8 for both ices VII and VIII. The slightly small value from the ideal number 2.0 would be ascribed to the systematic error related to the overall scaling of the scattering patterns, such as multiple scattering and attenuation. The molecular geometry of water in ice VII is hence identical to that in ice VIII (i.e., the apparently short O-D length in ice VII results from time average and spatial average in Rietveld analyses).

To compare interatomic correlations at longer distances, we discuss the pair distribution function $G(r)$ instead of $T(r)$. Fig. 3*C* shows that both ices VII and VIII have a peak at 0.97 Å, which corresponds to the O-D covalent bond as discussed for $T(r)$. On the other hand, the profiles differ from each other in t he region longer than the lattice parameter a_0 of ice VII. This means that ice VII does not have the same interatomic correlation as ice VIII over the distance of the second nearest neighbors. Especially, ice VIII has a tiny bump at 1.9 Å, which corresponds to hydrogen-bonded O … D, whereas that region in ice VII is smooth. Such difference in the correlation function is attributed to the molecular ordering in each phase. Based on a reported density functional theory–based calculation (23), local configurations like ice VIII are not dominant at pT conditions where ice VII is stable but other configurations have comparative populations. These are consistent with the atomic distribution obtained from the MEM analysis in which <100> displacements are not observed.

Discussion

The atomic distribution observed in the MEM analyses would reflect the dynamic nature of ice VII. The total scattering analyses revealed that the water molecule has a chemically plausible geometry in ice VII, as expected in the case of ice I_h (21). The disorder comprises the molecular orientation and their displacements from the average positions, resulting in the unusual atomic arrangements of ice VII described by the discrete atomic

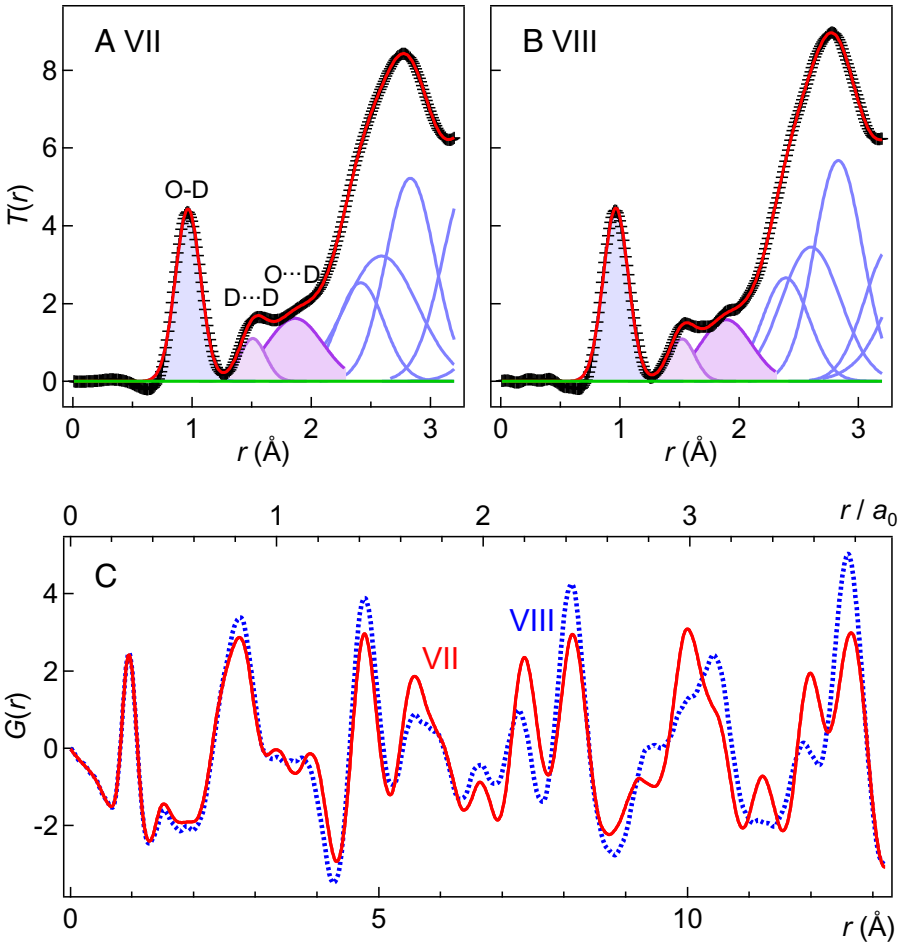

Fig. 3. Total correlation functions $T(r)$ of (*A*) ice VII and (*B*) ice VIII at 274 K and 2.2 GPa. Each peak was fitted using Gaussian functions (blue curves). The black cross indicates measured data and the red line corresponds to a profile reproduced from peak fitting. The initial five peaks at $r < 2.5$ Å are located at the expected positions derived from the Rietveld analysis, whereas four peaks up to 4.4 Å were set to be at the maximal positions of the profile. (*C*) Pair distribution functions $G(r)$ of ice VII and VIII were obtained at 274 K and 2.2 GPa. The abscissa on top is normalized interatomic distance by lattice parameter a_0 = 3.346632 (13) Å of ice VII, determined from the Rietveld analysis.

sites in the single-site and multi-site models in conventional structure analyses. Spectroscopic studies (24–26) and the quick transformation from ice VIII to ice VII (2) imply that the disordering of ice VII takes place dynamically at around 300 K. The atomic distribution is related to such dynamic conversion among the configurations. The dynamic motions in ice are expressed mainly by two components, rotation and translation. Their contributions depend on pressure in a contrasting way. At lower pressures, water molecules have enough space to flip, and rotation motion is dominant. Under higher pressure, the water molecules get closer and become difficult to flip. On the other hand, reducing the intermolecular distances enhances the probability of translation of deuterium between neighboring water molecules. The crossover of two dynamics takes place at approximately 10 GPa, first suggested from Raman spectroscopy (1) and recently proven from dielectric measurements (27), and illustrates the origin of previously reported anomalies, such as peak widths of stretching mode (1), phase transition kinetics (2), electrical conductivity (25), and proton diffusion (26). In conventional structure refinements, ADPs decrease with increasing pressure ($2 < P < 10$ GPa) and become almost constant above 10 GPa (8, 14, 28). This suggests that the atomic distribution in ice VII will be more localized up to 10 GPa. The localized distribution should be linked with the suppression of rotational motion.

The representation with two types of dynamic movement in ice VII introduces an aspect to attribute the observed unexpected distribution in ice VII to two features. First, the probability density is distributed in a ring-like shape around the <111> axes. Second, the deuterium also has elongated distribution toward the oxygen of hydrogen-bonded water. These distributions correspond to instantaneous deviation from the average position. The ring-like distribution should be related to a precession, assignable to rotational or librational motions of molecules, whereas the elongation along the hydrogen bond would correspond to the translational motion of deuterium approaching the hydrogen-bonded neighboring molecule.

In addition to the dynamic nature of ice VII, static configurations also play important roles in the disordered structure of ice VII. The phase-transition boundary between ices VII and VIII are almost temperature independent below 10 GPa, consistent with an estimation from the Clapeyron equation ($dp/dT = \Delta S/\Delta V$) with their little volume difference, ~5 mm^3/mol compared with the Pauling entropy, 3.37 J/(K·mol). On the other hand, the boundary slope becomes steeper at higher pressures, suggesting that the volume change between ices VII and VIII is significant in this pressure regime. Ab initio calculation estimated the energy gaps among molecular configurations to be the smallest at this pressure regime, reproducing the tendency of the order–disorder phase boundary between ices VII and VIII (23). Our total

Table 1. Summary of interatomic distances derived from Gaussian peak fitting of correlation function $T(r)$ and Rietveld refinement, with reported values

		$VII_{T(r)}$	$VIII_{T(r)}$	VII_{Riet}	$VIII_{Riet}$	VIII	VIII
	unit	This study				ref. 10	ref. 11
r(O-D)	Å	0.9662 (5)*	0.9658 (5)*	0.9163 (5)†	0.9681 (8)†	0.968 (7)†	0.973 (11)†
r(D ... D)	Å	1.510 (5)*	1.521 (6)*	1.4963 (10)†	1.5498 (14)†	1.543 (14)†	1.532 (12)†
r(O ... D)	Å	1.86 (13)*	1.89 (26)*	1.9820 (5)†	1.9304 (8)†	1.911 (9)†	1.920 (10)†
∠DOD	°	102.8 (4)*	103.9 (6)*	109.47	106.34 (11)†	105.6 (11)†	103.8 (15)†
p	GPa	2.2	2.2	2.2	2.2	2.4	2.8
T	K	274	274	274	274	10	269

*Errors estimated from the SD of peak fitting for $T(r)$ are given in parentheses.
†Errors estimated from the refinement procedures are given in parentheses. Riet, Rietveld.

scattering analysis revealed the clear difference in intermolecular structures of the disordered phase from the ordered counterpart. Further investigation at higher pressures can provide direct evidence for the pressure-dependent variation of the local structure as a result of the probability of dominant configurations. Moreover, the turning pressure overlaps with where the crossover of dynamics occurs (27). Fundamental and detailed diffraction techniques can provide direct and pivotal information on the anomalous physical properties of ice VII under pressure.

Our findings would also provide an approach to elucidate the behaviors of water molecules during the phase transition to hydrogen-bond symmetrized ice X. Although spectroscopic studies showed in the 1990s that ice VII transforms into ice X at greater than 60 GPa in H_2O and 70 GPa in D_2O (29–31), the symmetric structure of ice X has not been confirmed experimentally yet by neutron diffraction. A powder neutron-diffraction study of D_2O up to 60 GPa reported the elongation of covalently bonded O-D separation (28). The separation of the deuterium site between the hydrogen-bonded water molecules also decreases, and its linear extrapolation proposed an upper limit of the symmetrization to be at 113 GPa. Below 60 GPa, water is considered to retain its molecular nature, from spectroscopic studies (29–31), but the physical properties of the BCC ice differ from ice VII (32–34), called ice VII′. In this pressure regime, the bimodal potential curve of deuterium becomes unimodal, and quantum tunnelling dominates. The atomic distribution and the correlation function can provide direct images to observe the transient states toward the hydrogen-bond symmetrization.

Materials and Methods

Single-Crystal Neutron Diffraction. The single-crystal diffraction experiment was conducted at the D9 hot neutron single-crystal diffractometerat the Institut Laue-Langevin. The data on ice VII were collected at 298 K and 2.2 GPa using a diamond anvil cell specially designed for this study (35). Single-crystalline specimens of deuterated ice VII were grown directly from a water–alcohol mixture (D_2O:MeOD:EtOD = 5:4:1 in volume ratio) by cyclic heating and cooling over 2 GPa. The pressure was estimated by the ruby fluorescence method (36).

Powder Neutron Diffraction. The powder diffraction experiments were conducted at the BL11 (PLANET) beamline (18) of the Material and Life Science Experimental Facility at J-PARC using the MITO pressure–temperature variable system (37). Powder samples of deuterated ice VII were obtained by compression of ice at 200 K, below the melting curve of ice phases. The repetitive solid–solid phase transition contributes to preparing fine-powder samples suitable for structure analyses. The diffraction patterns of ice VII were collected at 2.2 GPa and temperatures of 298 K and 274 K. A powder diffraction pattern of ice VIII was also collected at 274 K and 2.2 GPa for comparison. The sample pressures were estimated from the equation of state of ice VII and VIII themselves (8). The phase transition between ices VII and VIII is a first-order transition that shows hysteresis so that both phases can metastably exist at ∼274 K during cooling for ice VII or heating for ice VIII before the phase transition occurs.

MEM Analysis. The MEM analysis tends to give the most uniform distribution under conditions that satisfy the constraints. The information entropy S, and the constraints C are defined as follows:

$$S = -\sum_{\boldsymbol{r}}^{\text{unit cell}} \rho(\boldsymbol{r}) \ln\left(\frac{\rho(\boldsymbol{r})}{\tau(\boldsymbol{r})\sum_{\boldsymbol{r}}^{\text{unit cell}}\rho(\boldsymbol{r})}\right), \quad [1]$$

$$C = \frac{1}{N_k}\sum_{\boldsymbol{k}}\left|\frac{F_0(\boldsymbol{k}) - F_c(\boldsymbol{k})}{\sigma F_0(\boldsymbol{k})}\right|^2 - 1, \quad [2]$$

where $\rho(\boldsymbol{r})$ is the normalized density of scattering length at $\boldsymbol{r}$ in a unit cell and $\tau(\boldsymbol{r})$ is the normalized density derived from prior information for $\boldsymbol{r}$, N_k is the number of structure factors, $\boldsymbol{k}$ is the reciprocal lattice vector to identify each Bragg reflection, and F_c is the structure factors calculated from $\rho(\boldsymbol{r})$. The most probable density distribution which maximizes S can be derived by a method of undetermined Lagrange multipliers (λ and μ), as follows:

$$Q = S - \lambda C - \mu\left(\sum_{\boldsymbol{r}}^{\text{unit cell}}\rho(\boldsymbol{r}) - 1\right), \quad [3]$$

The third term in Eq. 3 is a constraint for the total normalized scattering length to be one. The MEM analyses for both single-crystal and powder diffraction were done using the *Dysnomia* program (38), and the practical and detailed schemes are in its manual. The crystal structures and density distribution map were drawn with the *VESTA* program (39).

Total Scattering Analysis. Structure factors, $S(Q)$, were derived after intensity corrections for background, absorption, etc. $S(Q)$ is related to the atomic pair distribution function $g(r)$ by Eq. **4**. Derived correlation functions were analyzed in the forms of the total correlation function $T(r)$ and the pair-distribution function $G(r)$, defined by Eqs. **5** and **6**.

$$Q[S(Q) - 1] = \int_0^\infty 4\pi\rho_0 r[g(r) - 1]\sin(Qr)dQ \quad [4]$$

$$T(r) = 4\pi r\rho_0 g(r) \quad [5]$$

$$G(r) = 4\pi r\rho_0(g(r) - 1) \quad [6]$$

Data Availability. All study data are included in the article and/or supporting information.

ACKNOWLEDGMENTS. This study was supported by Japan Society for the Promotion of Science (JSPS) Grants-in-Aid for Scientific Research (grants 18H05224, 18H01936, and 21K18154), JSPS-CNRS bilateral joint research grant PRC2191, and the Global Institute for Materials Research Tohoku program of the Institute for Materials Research, Tohoku University (proposal 20K0085). Neutron diffraction experiments were performed through the J-PARC user programs (no. 2020B0139) and the Institut Laue-Langevin user programs (no. 5-15-624). The experiment at the J-PARC was performed using the Laboratory III at the Comprehensive Research Organization for Science and Society (CROSS) user

laboratory. We acknowledge an important contribution of J. S. Loveday which explains and clarifies our findings on the total scattering analysis.

Author affiliations: [a]Geochemical Research Center, Graduate School of Science, The University of Tokyo, Bunkyo-ku 113-0033, Japan; [b]Institut de Minéralogie, de Physique des Matériaux et de Cosmochimie, CNRS UMR 7590, Sorbonne Université, Muséum National d'Histoire Naturelle, F-75252 Paris, France; [c]Institut Laue-Langevin, F-38042 Grenoble Cedex 9, France; [d]Neutron Science and Technology Center, Comprehensive Research Organization for Science and Society, Tokai, Naka 319-1106, Japan; [e]J-PARC Center, Japan Atomic Energy Agency, Tokai-mura 319-1195, Japan; [f]Geodynamics Research Center, Ehime University, Matsuyama 790-8577, Japan; and [g]Institute for Materials Research, Tohoku University, Aoba-ku 980-8577, Japan

1. P. Pruzan, J. C. Chervin, M. Gauthier, Raman spectroscopy investigation of ice VII and deuterated ice VII to 40 GPa. Disorder in ice VII. *Europhys. Lett.* **13**, 81–87 (1990).
2. K. Komatsu *et al.*, Anomalous hydrogen dynamics of the ice VII-VIII transition revealed by high-pressure neutron diffraction. *Proc. Natl. Acad. Sci. U.S.A.* **117**, 6356–6361 (2020).
3. T. Iitaka, Simulating proton dynamics in high-pressure ice. *Rev. High Press. Sci. Technol. No Kagaku To Gijutsu* **23**, 124–132 (2013).
4. M. Benoit, D. Marx, M. Parrinello, Tunnelling and zero-point motion in high-pressure ice. *Nature* **392**, 258–261 (1998).
5. M. Benoit, D. Marx, M. Parrinello, Quantum effects on phase transitions in high-pressure ice. *Comput. Mater. Sci.* **10**, 88–93 (1998).
6. S. W. Peterson, H. A. Levy, A single-crystal neutron diffraction study of heavy ice. *Acta Crystallogr.* **10**, 70–76 (1957).
7. E. Whalley, D. W. Davidson, J. B. R. R. Heath, Dielectric properties of ice VII. Ice VIII: A new phase of ice. *J. Chem. Phys.* **45**, 3976–3982 (1966).
8. S. Klotz *et al.*, Bulk moduli and equations of state of ice VII and ice VIII. *Phys. Rev. B* **95**, 174111 (2017).
9. K. Komatsu *et al.*, Crystal structure of magnesium dichloride decahydrate determined by X-ray and neutron diffraction under high pressure. *Acta Crystallogr. B Struct. Sci. Cryst. Eng. Mater.* **71**, 74–80 (2015).
10. W. F. Kuhs, J. L. Finney, C. Vettier, D. V. Bliss, Structure and hydrogen ordering in ices VI, VII, and VIII by neutron powder diffraction. *J. Chem. Phys.* **81**, 3612–3623 (1984).
11. J. D. Jorgensen, R. A. Beyerlein, N. Watanabe, T. G. Worlton, Structure of D_2O ice VIII from in situ powder neutron diffraction. *J. Chem. Phys.* **81**, 3211–3214 (1984).
12. J.-L. Kuo, M. L. Klein, Structure of ice-VII and ice-VIII: A quantum mechanical study. *J. Phys. Chem. B* **108**, 19634–19639 (2004).
13. J. D. Jorgensen, T. G. Worlton, Disordered structure of D_2O ice VII from in situ neutron powder diffraction. *J. Chem. Phys.* **83**, 329–333 (1985).
14. R. J. Nelmes, J. S. Loveday, W. G. Marshall, G. Hamel, J. M. Besson, Multisite disordered structure of ice VII to 20 GPa. *Phys. Rev. Lett.* **81**, 2719–2722 (1998).
15. J. C. Li, M. Adams, Inelastic incoherent neutron scattering study of the pressure dependence of ice VII and VIII. *Europhys. Lett.* **34**, 675–680 (1996).
16. S. Klotz, T. Strässle, C. G. Salzmann, J. Philippe, S. F. Parker, Incoherent inelastic neutron scattering measurements on ice VII: Are there two kinds of hydrogen bonds in ice? *Europhys. Lett.* **72**, 576–582 (2005).
17. C. Knight, S. J. Singer, Site disorder in ice VII arising from hydrogen bond fluctuations. *J. Phys. Chem. A* **113**, 12433–12438 (2009).
18. T. Hattori *et al.*, Design and performance of high-pressure PLANET beamline at pulsed neutron source at J-PARC. *Nucl. Instruments Methods Phys. Res.* **780**, 55–67 (2015).
19. P. Loubeyre, R. LeToullec, E. Wolanin, M. Hanfland, D. Husermann, Modulated phases and proton centring in ice observed by X-ray diffraction up to 170 GPa. *Nature* **397**, 503–506 (1999).
20. M. Somayazulu *et al.*, In situ high-pressure x-ray diffraction study of H_2O ice VII. *J. Chem. Phys.* **128**, 064510 (2008).
21. M. A. Floriano *et al.*, Direct determination of the intramolecular O-D distance in ice Ih and Ic by neutron diffraction. *Nature* **329**, 821–823 (1987).
22. M. Guthrie *et al.*, The local structure of ice VII determined by neutron total scattering. *Acta Crystallogr. A* **61**, c94 (2005).
23. K. Umemoto, R. M. Wentzcovitch, S. de Gironcoli, S. Baroni, Order–disorder phase boundary between ice VII and VIII obtained by first principles. *Chem. Phys. Lett.* **499**, 236–240 (2010).
24. E. Katoh, H. Yamawaki, H. Fujihisa, M. Sakashita, K. Aoki, Protonic diffusion in high-pressure ice VII. *Science (80-.)* **295**, 1264–1266 (2002).
25. T. Okada, T. Iitaka, T. Yagi, K. Aoki, Electrical conductivity of ice VII. *Sci. Rep.* **4**, 5778 (2014).
26. N. Noguchi, T. Okuchi, Self-diffusion of protons in H_2O ice VII at high pressures: Anomaly around 10 GPa. *J. Chem. Phys.* **144**, 234503 (2016).
27. R. Yamane, K. Komatsu, H. Kagi, Direct evidence of the proton-dynamics crossover in ice VII from high-pressure dielectric measurements beyond 10 GPa. *Phys. Rev. B* **104**, 214304 (2021).
28. M. Guthrie *et al.*, Structure and disorder in ice VII on the approach to hydrogen-bond symmetrization. *Phys. Rev. B* **99**, 184112 (2019).
29. K. Aoki, H. Yamawaki, M. Sakashita, H. Fujihisa, Infrared absorption study of the hydrogen-bond symmetrization in ice to 110 GPa. *Phys. Rev. B Condens. Matter* **54**, 15673–15677 (1996).
30. A. F. Goncharov, V. V. Struzhkin, M. Somayazulu, R. J. Hemley, H. Mao, Compression of ice to 210 gigapascals: Infrared evidence for a symmetric hydrogen-bonded phase. *Science (80-.)* **273**, 218–220 (1996).
31. P. Pruzan *et al.*, Raman scattering and X-ray diffraction of ice in the megabar range. Occurrence of a symmetric disordered solid above 62 GPa. *J. Phys. Chem. B* **101**, 6230–6233 (2002).
32. A. Polian, M. Grimsditch, New high-pressure phase of H_2O: Ice X. *Phys. Rev. Lett.* **52**, 1312–1314 (1984).
33. E. Sugimura *et al.*, Compression of H_2O ice to 126 GPa and implications for hydrogen-bond symmetrization: Synchrotron x-ray diffraction measurements and density-functional calculations. *Phys. Rev. B Condens. Matter Mater. Phys.* **77**, 214103 (2008).
34. A. S. J. Méndez *et al.*, Bulk modulus of H_2O across the ice VII-ice X transition measured by time-resolved x-ray diffraction in dynamic diamond anvil cell experiments. *Phys. Rev. B* **103**, 1–7 (2021).
35. K. Yamashita *et al.*, A nano-polycrystalline diamond anvil cell with bulk metallic glass cylinder for single-crystal neutron diffraction. *High Press. Res.* **40**, 88–95 (2020).
36. H. Mao, J. Xu, P. M. Bell, Calibration of the ruby pressure gauge to 800 kbar under quasi-hydrostatic conditions. *J. Geophys. Res.* **91**, 4673 (1986).
37. K. Komatsu *et al.*, Development of a new P-T controlling system for neutron-scattering experiments. *High Press. Res.* **33**, 208–213 (2013).
38. K. Momma, T. Ikeda, A. A. Belik, F. Izumi, Dysnomia, a computer program for maximum-entropy method (MEM) analysis and its performance in the MEM-based pattern fitting. *Powder Diffr.* **28**, 184–193 (2013).
39. K. Momma, F. Izumi, VESTA 3 for three-dimensional visualization of crystal, volumetric and morphology data. *J. Appl. Cryst.* **44**, 1272–1276 (2011).